RSC Advances

RSC Advances

www.rsc.org/advances

ROYAL SOCIETY
OF CHEMISTRY

www.rsc.org/advances

Enhanced Microwave Absorption Properties of Ferroferric Oxide/ Graphene composites

with Controllable Microstructure

Rui Zhang[a], Xiaoxiao Huang[a*], Bo Zhong[b], Long Xia[b], Guangwu Wen[a,b],Zhou Yu[a],

[a] School of Materials Science and Engineering, Harbin Institute of Technology, Harbin 150001,

China

[b] School of Materials Science and Engineering, Harbin Institute of Technology at Weihai, Weihai

264209, China

Abstract

Fe_3O_4/graphene composites were synthesized as an advanced electromagnetic wave

absorption material by a solvothermal method in the system of ethylene glycol. The

Fe_3O_4 nanoparticles were homogeneously anchored on the graphene sheets and the

structures of the nanoparticles could be experimentally controlled from ring-like

spheres, flower-like spheres to solid spheres by changing the concentration of the

oxide graphene. Microwave absorption tests demonstrated that the structures of the

nanoparticles had a positive influence on the microwave absorption properties.

Especially, for the Fe_3O_4/graphene composite with the flower-like structure, the

minimum reflection loss value (RL) could reach -53.2 dB and the bandwidth of RL

less than 10 dB (90% absorption) ranged from 8.1 to 16 GHz at the thickness of

2.5mm, which is among the best-reported performances of Fe_3O_4/graphene materials,

showing the huge potential to be used as a kind of candidate for microwave absorbing

materials.

∗Corresponding author Tel: +86-451-86418694　Fax：+86-451-86413922
Email address: swliza@hit.edu.cn(XX.Huang)

Introduction

In recent decades, electromagnetic wave absorption (EMA) materials have received

much attention due to the urgent requirements in the fields of electrical apparatus,

information technology, human health[1] and military equipment[2]. Generally, the EMA

materials can be classified into two kinds: one is dielectric loss material like carbon

nanotubes and conductive polymers[3-5], the other is magnetic loss material such as Ba

M-type ferrite[6] , Ni, and so on. Among the latter, ferroferric oxide (Fe_3O_4)

nanoparticle, one of the typical ferromagnetic materials, is considered as an ideal

microwave absorption material due to the low cost, excellent magnetic properties,

non-toxicity, high compatibility and morphology controllability[7, 8]. However, the use

of nanoparticles in microwave absorption has some limitations, typically related to the

high density and easy agglomeration. In order to improve the EMA properties, a

variety of strategies as following have been applied to the Fe_3O_4 nanoparticles: (1) the

Fe_3O_4 nanoparticles coated with graphitic or non-graphitic carbon (carbon[9], carbon

nanohorns[10] and graphene[11, 12]); (2) Fe_3O_4 based composite architectures (other metal

oxide[13] and conductive macromolecule[14]); (3) unique Fe_3O_4 nanostructure

/microstructure with hollow hemispheres[15], bowl like[16] and porous hollow beads[17]. In

these strategies mentioned above, Fe_3O_4/graphene composites have been developed to

provide outstanding electromagnetic property.

Graphene, a newfound carbon material with the structure of sp^2 carbon atoms tightly

packed into a honeycomb network, has been regarded as an ideal component of the

EMA materials due to its large specific surface area (2630 m^2/g), excellent electronic

mobility (2×10^5 cm^2/V$^.$S), thermal conductivity (5000 W/m$^.$K), and mechanical strength (Yong's modulus, 1100 GPa)[18]. According to the previous reports about microwave absorbers, many effective efforts have been focused on compositing graphene with nitrile butadiene rubber[19], Ni[20, 21], Co_3O_4[22], SiO_2[23] macromolecule[24], polyaniline-gold[25] and so on. In these composites, the ultrathin flexible graphene sheets can provide a substrate to anchor the nanoparticles, and prevent the agglomeration of nanoparticles. Besides, the good impedance match characteristic also contributes to improve their EMA properties. Therefore, graphene-based magnetic hybrids are believed to be an ideal component in the EMA materials. Previous literatures[26-28] about the Fe_3O_4/graphene (or reduced graphene oxide) composites also indicated that the EMA properties have been improved compared with Fe_3O_4 nanoparticles or graphene alone. For example, Hu et sl.[29] reported the 3D graphene-Fe_3O_4 composites exhibited the calculated minimum RL about -27 GHz with a thickness of 2mm ; Li et sl.[28] exhibited the maximum reflection loss value of -30.1dB at a 1.48mm and 17.2GHz matching   frequency. But all of them researched only on one single morphology of the nanoparticles, and the researches about the morphology controllability of Fe_3O_4 nanoparticles as well as the effect of the nanostructures on the EMA properties are rare.

In this article, Fe_3O_4/graphene composites are fabricated by a facile solvothermal method. The Fe_3O_4 nanoparticles with different size, bearing capacities and morphologies are uniformly spread over graphene sheets, and the influence of the controllable morphology on the EMA properties has been systematically studied.

Consequently, through changing the mass ratio of the raw materials, the morphology of Fe_3O_4 nanoparticles could be easily controlled and changed from the ring-like spheres, flower-like spheres to solid spheres. Specially, the composite with flower-like particles which shows the optimum properties of high absorbing intensity, wide absorption frequency, thin thickness and light density. The outstanding properties highlight the great potential of Fe_3O_4/graphene composites as promising materials for lightweight and high performance absorbers.

Experimental

Fabrication of the Fe_3O_4/graphene composites

The graphene oxide (GO) was synthesized through a modified Hummer's method[30]. The Fe_3O_4 /graphene composites were fabricated in ethylene glycol. In a typical experiment, the ground GO powder was dissolved in 30 ml ethylene glycol (concluding 0.75 ml deionized water) with ultrasonic dispersion for 3 hours, and then 0.54 g $FeCl_3·6H_2O$ and 1.05 g urea were added into the solution and mixed uniformly. Next, the solution was transferred into a 50 ml Teflon-lined autoclave and maintained at 200℃ for 14 h. Subsequently, the products were washed with deionized water and ethyl alcohol by centrifugation. Fe_3O_4/graphene composites with different mass ratio of GO and Fe_3O_4 nanoparticles ($M_{GO}:M_{Fe3O4}$) were obtained and labeled as Sample 1(1:1), Sample 2 (5:1), Sample 3 (10:1) and Sample 4 (20:1). The pure Fe_3O_4 nanoparticles are synthesized with the same method without GO.

Characterization

The morphologies of the as-synthesized samples were characterized by the scanning

electronic microscopy (SEM, FEI-Quanta 200F), and transmission electron microscopy (TEM, JEOL210- FEI Tecnai G^2 F30 at 300 KV). The powder X-ray diffraction (XRD) patterns were recorded on Rigaku D/max-γ B X-ray diffractometer using Cu Kα radiation. X-ray photoelectron spectroscopy (XPS) studies were performed using the Thermo Fisher 0ESCALAB 250Xi. Raman studies of randomly oriented samples were performed with a Renishaw Ramoscope (Confocal Raman Microscope, in Via, Renishaw). The magnetic hysteresis loops were performed by a vibrating sample magnetometer (VSM, SQUID-VSM) at room temperature. Thermal gravimetric analysis was performed on a thermal analyzer (Mettler-Toledo TGA/SDTA851e) from room temperature to 800℃ in air at a heating rate of 10℃ min^{-1}. The electromagnetic parameters of complex magnetization and complex permeability were investigated by Vector Network Analyzer, Agilent, N5230A. The samples were prepared by evenly mixing the product with a paraffin max in mass fraction of 1:4 and then being pressed into a toroidal-shaped special stainless steel mould with the inner and outside diameters of 3 and 7 mm, respectively.

Results and discussion

Microstructure, chemical analysis and morphology of Fe$_3$O$_4$/graphene composites

Fig. 1(a) shows the XRD of the GO, graphene and Fe$_3$O$_4$/graphene composites. Because of the oxidation, the GO shows a sharp diffraction peak at 11.6º, corresponding to a larger basal spacing of 0.74 nm. The characteristic diffraction peak of graphene reduced by ethylene glycol presents a weak and broad diffraction peak approximately at 24º, which proves the removing of oxygen-containing groups and

disordered stacking of single graphitic sheets. A cubic structure phase for Fe_3O_4 in the composites is confirmed by XRD with well-defined diffraction peaks at pattern of 30.1, 35.45, 43.1, 53.5, 56.9 and 62.57° corresponding to (220), (311), (400), (422), (511) and (440) lattice planes (JCPD card No.65-3107) without any impurity phases (Fig.1 (a) and Fig. S1). Besides, because of the overlapping of graphitic layers, the peaks become weaker for Fe_3O_4 nanoparticles while sharper for the graphite from Sample 1 to Sample 4 shown in Fig.1a. It indicates that the nanoparticles could prevent the stacking of carbon layers. Raman spectra analysis shown in Fig. 1(b) further indicates the reduction of the GO and the appearance of the Fe_3O_4 particles in the composites. Raman spectrum of GO and Sample 1 display a prominent G-band (1599 cm^{-1}) along with D-band (1352 cm^{-1}), and the D/G intensity ratio increases from 0.89 for GO to 1.26 for Sample1. This means that the decrease in the average size of the sp^2 domains [31] and the removing of most oxygen-containing groups. Additionally, the Raman bands for Sample1 at 224.6 and 493.1 cm^{-1} correspond to the A_{1g} mode and the bands at 291.4, 406.9 and 608.3 cm^{-1} could be attributed to the E_g mode of Fe_3O_4, which are consistent with the results in XRD patterns.

To investigate the chemical compositions of Fe_3O_4/graphene composites, XPS were carried out as shown in Fig. 2. In the XPS spectra of Sample 1, the C_{1s} peak at 284.7 eV contains three kinds of components, arising from C-C/C=C in the graphitic carbon, C-O in the residual oxygen-containing groups and C-N due to the N doped on the graphitic layers , respectively[32] (Fig. 2b). The O_{1s} peak at 531.3 eV can be fitted to four peaks (O-C-O, Fe-O, Fe-O-C, and C-O peak), which mainly come from the

Fe_3O_4 and residual oxygen groups (Fig. 2c). Noteworthily, the Fe-O-C bond at 530.3 eV proves the strong chemical connection between the Fe_3O_4 and graphitic carbon. Furthermore, two peaks at 711.1 eV and 724.8 eV corresponding to the band energies of $Fe_{2p3/2}$ and $Fe_{2p1/2}$, respectively, indicate the formation of a mixed oxide of Fe(II) and Fe(III), and further confirm the existence of Fe_3O_4 nanoparticles.

SEM and TEM are used to investigate the microstructure of the products. Fig. S2a is the representative view of the graphene with a crumple structure. The ring-like spheres Fe_3O_4 nanoparticles with an average diameter of 200 nm and a shell thickness of 50 nm are uniformly deposited on the graphitic sheets in Sample 1 as shown in Fig. 3a and 3b. They are different from the pure Fe_3O_4 nanoparticles which present hollow structures with a diameter of about 200 nm and a shell thickness of 50 nm (Fig. S2 (b) and Fig.S3-S5). Fig. 3b further indicates that all the Fe_3O_4 nanoparticles are homogenously embedded on the wrinkle graphene sheets. The HRTEM image and the SAED pattern presented in the Fig. 3c clearly demonstrate the single crystalline structure of Fe_3O_4 nanoparticles in the composites.

The Sample 2 and Sample 3 present distinct flower-like spheres with a size of about 50 nm in Fig.4. More nanoparticles are assembled on the graphene sheets in Sample 2 than Sample 3 (Fig. 4a-d). This means it is easy to control the loading amount and morphology of nanoparticles on the graphene sheets by altering the mass ratio of reagents. Fig. 4e and 4f present the TEM and HRTEM images of the flower-like composites. The uniform Fe_3O_4 nanoparticles are deeply and firmly embedded on the graphene sheets. As shown in Fig. 4f, the crystal lattice fringes with a spacing of

0.253 nm and 0.297 nm are assigned to the (311) and (220) plane of the Fe_3O_4 crystal, respectively, which are consistent with the results of Fig. 1(a). Besides, the small cluster of the Fe_3O_4 is constructed with many small Fe_3O_4 nanoparticles with diameters ranging from 10 to 25 nm. Fig. S6 shows the morphology of the composites Sample 4 with solid Fe_3O_4 sphere. Few Fe_3O_4 nanoparticles are anchored on the carbon sheets because of the huge mass ratio, and this also indicates the controllability of the loading amount and morphology of nanoparticles.

Several characteristics of the composites should be mentioned: (1) it is easy to control the morphology of the nanoparticles from the ring-like sphere, flower-like structure to the solid sphere with the increase of reactants ratio; (2) the nanoparticles firmly attached on the carbon layers after a powerful sonication treatment during the preparation of TEM samples. This shows the strong connection between the carbon and the nanoparticles, which are consistent with the results of XPS; (3) it is noteworthy that the flower-like nanoparticles on graphene sheets have smaller size and more interfaces than the ring-like spheres in Sample 1 or the solid spheres in Sample 4, which may have strong influence on the EMA properties due to the interface loss.

Fig.5 shows the possible evolution process of Fe_3O_4/graphene composites. The GO can attract the Fe^{3+} and Fe^{2+} due to the electrostatic interaction between the oxygen-containing groups and iron ions. In this process, some ferric ions connect with the oxygen-containing groups linked to the carbon layers, the others connect with the free oxygen-containing groups in the solution. Accordingly, two kinds of Fe_3O_4

nanoparticles are fabricated, as shown in Fig.5 (a). However, the growth of the two kinds of nanoparticles is not synchronous: the nanoparticles which are not linked on the graphitic layer grow up sharply, while the growth of the nanoparticles connected on the carbon layers is limited. Meanwhile, with increasing time, the reduction of the GO and the growth of Fe_3O_4 happened simultaneously (Fig. S7). Consequently, the Fe_3O_4/graphene composites are fabricated by the easy solvothermal process.

Based on the analysis above, the possible fabricated processes are shown in the Fig.5b~d. In Sample 1 plentiful iron ions can unite together to form spheres and then evolve into ring-like structures driven by the minimization of interfacial energy and magnetic dipole interaction (shown in Fig. 5 b). In Sample 2 and Sample 3, the quantity of the oxygen-containing groups increases compared with Sample 1, and the interactions between the ions and these groups are stronger than those between ions themselves. In another words, the excess groups restrict the growth and the self-assembly of Fe_3O_4 nanoparticles, which can only combine with some nearby small size atoms to form flower-like structure. Moreover, with further increasing of the GO mass ratio, the limited iron ions could just assemble on the edges and full defects areas and then form into solid spheres as shown in Fig.5d.

The magnetic properties of the composites and hollow Fe_3O_4 nanoparticles were examined at 300K shown in Fig.6 (a). The magnetic hysteresis loops of the pure Fe_3O_4 nanoparticles and Sample 1, 2 and 3 composites show S-like shape to the curve and are ferromagnetic. The saturation magnetization values of these composites of are 37.1(sample 1), 10.4(sample 2), 4.7(sample 3) $emu.g^{-1}$, respectively, while that of

hollow Fe_3O_4 nanoparticles is 79 emug^{-1}. It indicates the saturation magnetization decreases with the increase of the mass ratio of graphene content. In sample 4, there is almost no magnetism because of the low levels of the Fe_3O_4 nanoparticles. And from fig.6, it indicates the magnetization of the composites is mainly related to the mass ratio of Fe_3O_4, and has little relationship with the morphology. Fig.6 (b) shows the TG curves of the products with different mass ratio. Thermograms of the composites show two major weight losses. The first is at about 100℃ which is due to the loss of water. The second is in the range of 370 to 500℃ and indicates the oxidization of graphene to CO_2 and the Fe_3O_4 to Fe_2O_3 in air[11]. When the temperature reached 800℃, the residue is Fe_2O_3 for all the composites. And the calculated Fe_3O_4 contents derived from the TG data are 51.71, 20.269, 13.6 and 7.39wt% for the corresponding graphene to Fe_3O_4 ratio of 1:1, 5:1, 10:1 and 20:1, respectively.

Microwave absorption properties of Fe_3O_4 /graphene composites

To evaluate the EMA properties, the complex permittivity and permeability of Fe_3O_4 nanoparticles, graphene, and Fe_3O_4/graphene composites are measured in the range of 2-18 GHz as shown in Fig.7.

The real parts of permittivity (ε') of graphene and composites (Sample 1, Sample 2, Sample 3, Sample 4) decline from 7.07 to 4.11,10.10 to 4.96, 11.19 to 5.6, 10.62 to 5.6 and 9.8 to 4.8 with the increasing frequency，respectively, while ε' for pure Fe_3O_4 nanoparticles indicates negligible change showing little dielectric properties[33, 34]. It is known that the ε' is associated with the amount of polarization in the absorber which mainly contain the dipolar polarization and interfacial polarization. And both these

two kinds of polarization mechanisms are more frequency-dependent. So the decrease

of the ε' for the composites may due to the decrease in space charge polarization with

increasing frequency[35]. Additionally, ε' increases with the increase of mass ration from

Sample 1 to Sample 3 but drops for Sample 4, while all the composites have a higher

value of ε' than Fe_3O_4 which may be caused by the different synergistic effect between

the graphene and Fe_3O_4 nanoparticles. As shown in the Fig. 7 b, the imaginary parts of

complex permittivity (ε'') exhibit a peak in the range of 10-17 GHz for the composites,

indicating a resonance behavior. While ε'' for pure Fe_3O_4 nanoparticles maintains a

low value and almost unchanged with increasing frequency. Because the complex

permeability contributes to the dielectric loss property[36], the value of ε'' of the

composites and graphene is higher than pure Fe_3O_4 nanoparticles, which suggests that

the electronic spin and charge polarization from the polarized centers have a great

effect on the EMA properties of the composites[32]. And the values of ε'' of sample2 and

3 are almost highest, which may due to the due to the flower-like morphology. The

real parts and imaginary parts of complex permeability (μ' and μ'') of the Fe_3O_4

nanoparticles, graphene and composites, are shown in Fig. 7 c and 7d. The values of

μ' fluctuate with a peak at 16 GHz for all the composites，may be caused by the eddy

current effect. The imaginary parts of complex permeability (μ'') also fluctuate around

-0.2~0.2 in the range of 2-18 GHz, indicating the surface effect and spin wave

excitations. Moreover, the value of μ'' exhibiting negative values under high

frequencies attributes to the motion of charges, which would generate an alternating

electromagnetic field[5].

Generally, Debye dipolar relaxation has an important influence on the EMA properties of dielectric absorbing materials. The relative complex permittivity can be expressed by the following equation[37],

$$\varepsilon_r = \varepsilon_\infty + \frac{\varepsilon_s - \varepsilon_\infty}{1 + j2\pi f \tau} = \varepsilon'(f) + i\varepsilon''(f) \tag{1}$$

Where f, ε_s, ε_∞, and τ are frequency, stationary dielectric constant, relative dielectric constant at the high-frequency limit, and polarization relaxation time, respectively. Thus, ε' and ε'' can be deduced from the previous expression by:

$$\varepsilon'(f) = \varepsilon_\infty + \frac{\varepsilon_s - \varepsilon_\infty}{1 + (2\pi f)^2 \tau^2} \tag{2}$$

$$\varepsilon''(f) = \frac{2\pi f \tau(\varepsilon_s - \varepsilon_\infty)}{1 + (2\pi f)^2 \tau^2} \tag{3}$$

The relationship between ε' and ε'' can be obtained from equations (2) and (3),

$$(\varepsilon' - \varepsilon_\infty)^2 + (\varepsilon'')^2 = (\varepsilon_s - \varepsilon_\infty)^2 \tag{4}$$

Thus, the plot of ε' versus ε'' would represent a single semicircle, generally denoted as the Cole–Cole semicircle, which corresponds to one Debye relaxation.

Fig. 8 shows the ε'-ε'' curve of pure Fe_3O_4 nanoparticles, graphene and composites. Two semicircles can be observed obviously in the ε'-ε'' curve of the composites (Sample 1 to Sample 4), while just an inconspicuous semicircle can be found in the pure Fe_3O_4 nanoparticles. This indicates that the graphene enhances the dielectric properties of the composites due to the double relaxation mechanism[3]. As previously mentioned in XPS and Raman analyses, there are many residual oxygen-containing groups and defects (such as lacking of carbon atoms, polyaromatic islands[38]) on the graphitic sheets, which can act as the polarization center. Additionally, the interfacial

polarization between the nanoparticles and the graphitic sheets also enhances the microwave loss[39]. So the increased relaxations for the composites compared with the pure Fe_3O_4, may arise from the interfacial polarizations between the nanoparticles and the graphene sheets, as well as the dipole polarizations induced by the residual oxygen-containing groups and defects[40]. Fig. 8b and 8c show the dielectric loss factor ($\tan\delta_\varepsilon = \varepsilon''/\varepsilon'$) and magnetic loss factor ($\tan\delta_\mu = \mu''/\mu'$) of the composites with different mass ratio. The values of $\tan\delta_\varepsilon$ increase from 2 to 16 GHz while decreases during higher frequencies for all the composites. Meanwhile, the composites have higher $\tan\delta_\varepsilon$ value than pure Fe_3O_4 nanoparticles, indicating a higher dielectric loss. Moreover, the values of $\tan\delta_\mu$ exhibit nonlinear change with increasing frequency. Obviously, the value of $\tan\delta_\varepsilon$ is higher than that for the $\tan\delta_\mu$, which means the dielectric loss play a greater role in the reflection loss of the Fe_3O_4/graphene composites.

According to the transmission line theory, the reflection loss (RL) of all products are calculated by the model of single absorber layer [41]:

$$Z_{in} = Z_0 (\frac{\mu_r}{\varepsilon_r})^{1/2} \tanh\left[\frac{j2\pi fd}{c}\left(\mu_r\varepsilon_r\right)^{1/2}\right] \quad (5)$$

$$R_L(dB) = 20\log\left|\frac{Z_{in}-1}{Z_{in}+1}\right| \quad (6)$$

Where f, d, c, Z_0 and Z_{in} are the frequency of electromagnetic wave, thickness of an absorber, the velocity of the light, the impedance of free space and the input impedance of the absorber, respectively, which are the determining factors of the

microwave absorption materials.

Fig. 9 show the calculated RL curves of Fe_3O_4 nanoparticles, graphene and Fe_3O_4/graphene composites with different thicknesses in the range of 2-18 GHz. The pure Fe_3O_4 nanoparticles with a hollow structure have a weak RL value which does not exceed -10 dB (shown in Fig. 9a). While the graphene reduced from GO by ethylene glycol shows a good absorption for microwave with a minimum RL value of -35 dB at the thickness of 2 mm, which is different from the general result[42]. The interesting RL value of the graphene in our work may be caused by the residual oxygen-containing groups which can act as polarization center and so generate the polarization relaxation [42]. Fig. 9c shows the minimum RL value of -23.7 dB at 15.3 GHz (d=2.5 mm) and the bandwidth (RL< -10 dB) is about 6 GHz for Sample 1. It is also observed that the absorption peak shifts to the low frequency with the increase of absorber thickness corresponding to the quarter-wave principle[28]. Remarkably, sample 2 with the flower-like structure has the minimum RL of -53.2 dB at 11.4 GHz (d=2.5 mm) and the bandwidth of RL<-10 dB about 7 GHz which shows a better EMA properties than Sample 1 for the same thickness. It is almost the highest reflection absorption property ever reported for such composites[28, 43]. When the mass ratio increases further, for Sample 3 and Sample 4, the minimum values of RL are -45.3 dB at 13.5 GHz (d=2mm) and -40 dB at 11 GHz (d=2.5mm), respectively, and the ranges of RL< -10 dB widen with decreasing Fe_3O_4 nanoparticles loading. It is worth noting that Sample 3 (d=2.5 mm) has a RL value less than -10 dB which covers whole X-band (8-12 GHz) and this value for Sample 4 almost covers a majority of Ku-band

(12-18 GHz).It indicates that graphene can improve the microwave loss greatly, because of the connection of dielectric loss and magnetic loss. Compared with other works, the results in this work are better[10, 16, 44-48]. For example, Cui et sl.[10] reported the Fe_3O_4 decorated on the single-wall carbon nanoborns showing absorption bandwidth with 9.2 GHz (RL≤-10dB), but the max RL value only -38.8 dB. A higher max RL value was obtained with -53.5dB, but the reflection loss below -10dB (RL≤-10dB) only 2.8GHz in the PANI/GO/Fe_3O_4 composites[48]. Moreover the graphene-Fe_3O_4 nanohybrids[44] exhibited that the frequency range was 9.5GHz (from 5.1 to 14.6 GHz) for the reflection loss below -10dB, but the maximum reflection loss reaches -40.4dB at 7GHz for the absorber with thickness of 5mm.(Table 1). And in our work, the composites exhibit stronger and wider-frequency wave-absorbing properties.

From the results of the composites, it exhibits that when Fe_3O_4 nanoparticles adhere on the graphene layers uniformly, the dielectric constants and electromagnetic parameters can reach an appropriate value which would improve impedance matching and benefit to the microwave loss. Besides, from Fig. 9, we can obviously deduce that the microwave absorption properties could be adjusted by changing the mass ratio. Especially, the Sample 2 (flower-like structure) with the optimal ratio ($M_{GO}:M_{Fe_3O_4}$ =5:1) shows the strongest absorption (-53.2 dB) and a relative wide range (7GHz) of RL< -10 dB, which is attributed to the natural resonance mechanism and eddy current effect. As previously stated, the morphology of Fe_3O_4 nanoparticles changed with the increase of mass ratio from the ring- like sphere, to flower-like sphere and finally to

solid sphere. These structures have a crucial influence on the microwave absorption properties[16, 49]. From the fig-10, the schematic view indicates the relationship between the morphology and microwave absorption properties. The microwave absorption is mainly attributed to magnetic loss and dielectric loss, and the microwave is depleted as heat at last. In the sample 1 the ring-like Fe_3O_4 embedded in the graphene sheet, and the nature resonance and eddy current loss of the Fe_3O_4 lead to the loss of the microwave. And the interfacial polarization between the two phases can lead to an additional dielectric loss, but the microwave was limited in the hollow cavity by reflecting which confined the heat to the interior, and might weaken the absorption property. On the other hand, the sample 2 and sample 3 have an open structure, and the multi-interfaces between the flower-like sphere, graphitic sheets and paraffin matrix contribute to better properties due to the interfacial electric polarization which enhanced the loss of the microwave, and the heat dissipated through the graphene sheet. While comparing Sample 2 with Sample 3 which has both flower-like particles, we can notice that the RL value for Sample 2 is stronger than that for Sample 3, because appropriate amount of graphene can optimize the electromagnetic parameters and the impedance matching.

Conclusions

In this article, we reported a facile strategy to fabricate the Fe_3O_4/graphene composites with fantastic electromagnetic wave absorption properties. The structure of Fe_3O_4 nanoparticles is easily controlled from ring-like sphere, flower-like sphere to solid sphere with increasing mass ratio of GO and Fe^{3+}. The RL peaks of all the

composites moves to low frequency with increasing thickness. And the minimum RL value of the different mass ratio of Fe_3O_4/graphene composites are -25 dB at 17 GHz for Sample 1, -53.2 dB at 11 GHz for Sample 2, -45 dB at 13.5 GHz for Sample 3, and -40 dB at 11 GHz for Sample 4, respectively, which are much stronger than pure Fe_3O_4 nanoparticles. Furthermore, the optimal EMA material was obtained when the Fe_3O_4 nanoparticles are flower-like structure by controlling the mass ratio of the GO and Fe^{3+} (5:1), which makes the composite as excellent electromagnetic absorption materials at 2-18GHz.

SUPPORTING INFORMATION

XRD patterns of Fe_3O_4 nanoparticales (Figure S1), TEM images of nanoparticles of graphene and Fe_3O_4 (Figure S2), and SEM and TEM images of Sample 4(Figure S3), SEM images of Sample 1with different reaction time (Figure S4).

Acknowledgments

References

1.   F. S. Wen, H. Hou, J. Y. Xiang, X. Y. Zhang, Z. Y. Su, S. J. Yuan and Z. Y. Liu, *Carbon*, 2015, **89**, 372-377.

2.   D. Micheli, A. Vricella, R. Pastore and M. Marchetti, *Carbon*, 2014, **77**, 756-774.

3.   L. Kong, X. W. Yin, X. Y. Yuan, Y. J. Zhang, X. M. Liu, L. F. Cheng and L. T. Zhang, *Carbon*, 2014, **73**, 185-193.

4.   R. C. Che, L. M. Peng, X. F. Duan, Q. Chen and X. L. Liang, *Adv Mater*, 2004, **16**, 401-405.

5.   Mao-Sheng Cao, Jian Yang, Wei-Li Song, De-Qing Zhang, Bo Wen, Hai-Bo Jin, Zhi-Ling Hou and J. Yuan, *ACS Appl. Mater. Interfaces*, 2012, **4**, 6949-6956.

6.   R. S. Alam, M. Moradi, M. Rostami, H. Nikmanesh, R. Moayedi and Y. Bai, *J Magn Magn Mater*, 2015, **381**, 1-9.

7.   Z. M. Cui, L. Y. Jiang, W. G. Song and Y. G. Guo, *Chem. Mater.*, 2009, **21**, 1162-1166.

8.   J. Su, M. H. Cao, L. Ren and C. W. Hu, *J Mater Chem C*, 2011, **115**, 14469-14477.

9.   Longbin Cui, Yang Liu, Xiaohui Wu, Ziqi Hu, Zujin Shi, Huanjun Li and A Govindaraj, *RSC Adv.*, 2015, **5**, 75817-75822.

10.   Longbin Cui, Yang Liu, Xiaohui Wu, Ziqi Hu, Z. Shi and H. Li, *RSC Adv*, 2015, **5**, 75817-75822.

11.   J. Zheng, H. Lv, X. Lin, G. Ji, X. Li and Y. Du, *J Alloy Compd*, 2014, **589**, 174-181.

12.   Meng Zong, Ying Huang, Yang Zhao, Lei Wang, Panbo Liu, Yan Wang and Qiufen Wang, *Mater Lett*, 2013, **106**, 22-25.

13.   C. L. Zhu, M. L. Zhang, Y. Qia, G. Xiao, F. Zhang and Y. J. Chen, *J. Phys. Chem. C*, 2010, **114**, 16229-16235.

14.   P. B. Liu, Y. Huang and X. Zhang, *J Alloy Compd*, 2014, **617**, 511-517.

15.   J. P. Zou, Z. Z. Wang, M. Q. Yan and H. Bi, *J Phys D: Appl Phys* 2014, **47**, 275001.

16.   H. L. Xu, H. Bi and R. B. Yang, *J Appl Phys*, 2012, **111**, 07A522.

17.   Y. J. Zhang, S. Wing; and Z. D. Zhang, *J Nanosci Nanotechno*, 2014, **14**, 4664-4669.

18.   A. K. Geim and K. S. Novoselov, *Nat Mater*, 2007, **6**, 183-191.

19.   V. K. Singh, A. Shukla, M. K. Patra, L. Saini, R. K. Jani, S. R. Vadera and N. Kumar, *Carbon*, 2012, **50**, 2202-2208.

20.   T. T. Chen, F. Deng, J. Zhu, C. F. Chen, G. B. Sun, S. L. Ma and X. J. Yang, *J Mater Chem*, 2012, **22**, 15190-15197.

21.   G. Wang, Z. Gao, G. Wan, S. Lin, P. Yang and Y. Qin, *Nano Research*, 2014, **7**, 704-716.

22.   P. B. Liu, Y. Huang, L. Wang, M. Zong and W. Zhang, *Mater Lett*, 2013, **107**, 166-169.

23.   Bo Wen, Maosheng Cao, Mingming Lu, Wenqiang Cao, Honglong Shi, Jia Liu, Xixi Wang, Haibo Jin, Xiaoyong Fang, Wenzhong Wang and J. Yuan, *Adv. Mater.*, 2014, **26**, 3484-3489.

24.   Weilu Liu, Cong Li, Peng Zhang, Liu Tang, Yue Gu, Yujing Zhang, Jianqing Zhang, Zhongbo Liu, G. Sun and Z. Zhang，, *RSC Adv.*, 2015, **5**, 73993-74002.

25.   C. Basavaraja, W. J. Kim, Y. D. Kim and D. S. Huh, *Mater Lett* 2011, **65**, 3120-3123.

26.   J. Zheng, H. L. Lv, X. H. Lin, G. B. Ji, X. G. Li and Y. W. Du, *J Alloy Compd*, 2014, **589**, 174-181.

27.   M. Zong, Y. Huang, Y. Zhao, X. Sun, C. H. Qu, D. D. Luo and J. B. Zheng, *RSC Advances*, 2013, **3**, 23638-23648.

28.   X. H. Li, H. B. Yi, J. W. Zhang, J. Feng, F. S. Li, D. S. Xue, H. L. Zhang, Y. Peng and N. J. Mellors, *J Nanopart Res*, 2013, **15**, 1472.

29.   Chuangang Hu, Zhongyu Mou, Gewu Lu, Nan Chen, Zelin Dong, M. Hua and L. Qu, *Phys. Chem. Chem. Phys.*, 2013, **15**, 13038-13043.

30.   Y. Wen, Y. J. Zhu, A. Langrock, A. Manivannan, S. H. Ehrman and C. S. Wang, *Small*, 2013, **9**, 2810-2816.

31.   S. Stankovich, D. A. Dikin, R. D. Piner, K. A. Kohlhaas, A. Kleinhammes, Y. Jia, Y. Wu, S. T. Nguyen and R. S. Ruoff, *Carbon*, 2007, **45**, 1558-1565.

32.   D. C. Wei, Y. Q. Liu, Y. Wang, H. L. Zhang, L. Q. Huang and G. Yu, *Nano Lett*, 2009, **9**, 1752-1758.

33.   E. Ma, J. J. Li, N. Q. Zhao, E. Z. Liu, C. N. He and C. S. Shi, *Mater Lett*, 2013, **91**, 209-212.

34.   J. Qiu and T. T. Qiu, *Carbon*, 2015, **81**, 20-28.

35.   Kuldeep Singh, Anil Ohlan, Viet Hung Pham, Balasubramaniyan R., Swati Varshney, Jinhee Jang, Seung Hyun Hur, Won Mook Choi, Mukesh Kumar, S. K. Dhawan, Byung-Seon Kong and Jin Suk Chung, *Nanoscale*, 2013, **5**, 2411-2420.

36.   D. F. Zhang, F. X. Xu, J. Lin, Z. D. Yang and M. Zhang, *Carbon*, 2014, **80**, 103-111.

37.   H. L. Yu, T. S. Wang, B. Wen, M. M. Lu, Z. Xu, C. L. Zhu, Y. J. Chen, X. Y. Xue, C. W. Sun and M. S. Cao, *J Mater Chem*, 2012, **22**, 21679-21685.

38.   H. Hu, Z. B. Zhao, Q. Zhou, Y. Gogotsi and J. S. Qiu, *Carbon*, 2012, **50**, 3267-3273.

39.   SunGB, D. BX, C. MH, W. BQ and H. CW, *Chem Mater*, 2011, **23**, 1587-1593.

40.   L. Jia, C. Wenqiang, J. HaiBo, Z. Deqing and C. Maosheng, *Journal of Materials Chemistry C*, 2015, **3**, 4670-4677.

41.   X. G. Liu, D. Y. Geng, H. Meng, P. J. Shang and Z. D. Zhang, *Appl Phys Lett*, 2008, **92**, 173117.

42.   C. Wang, X. J. Han, P. Xu, X. L. Zhang, Y. C. Du, S. R. Hu, J. Y. Wang and X. H. Wang, *Appl Phys Lett*, 2011, **98**, 072906.

43.   T. Wang, Z. Liu, M. Lu, B. Wen, Q. Ouyang, Y. Chen, C. Zhu, P. Gao, C. Li, M. Cao and L. Qi, *J Appl Phys*, 2013, **113**, 024314.

44.   Tieshi Wang, Z. Liu, M. Lu, Bo Wen, Qiuyun Ouyang, Yujin Chen, Chunling Zhu, Peng Gao, Chunyan Li, Maosheng Cao and L. Qi, *J Appl Phys*, 2013, **113**, 024314.

45.   M. Jazirehpour and S. A. S. Ebrahimi, *Journal of Alloys and Compounds*, 2015   **638**, 188-196.

46.   Z. W. Li and Z. H. Yang, *J MAGN MAGN MATER*, 2015, **387**, 131-138.

47.   Meng Zong, Y. Huang, Yang Zhao, L. Wang, Panbo Liu, Yan Wang and Q. Wang, *Mater Lett*, 2013, **106**, 22-25.

48.   Jing Zhao, Junpin Lin, J. Xiao and H. Fan, *RSC Adv*, 2015, **5**, 19345-19352.

49.   R. F. Zhuo, H. T. Feng, J. T. Chen, D. Yan, J. J. Feng, H. d. J. Li, B. S. Geng, S. Cheng, X. Y. Xu and P. X. Yan, *J. Phys. Chem. C*, 2008, **112**, 11767-11775.
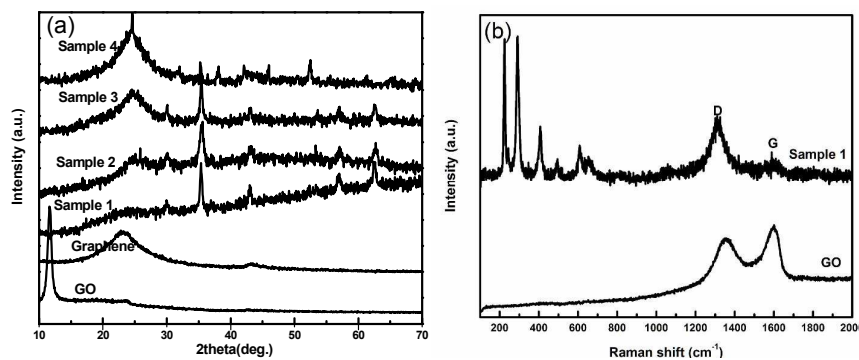
Fig.1- The chemical composition and crystal structure of Fe_3O_4 /graphene composites: (a) XRD patterns of GO, graphene and Fe_3O_4 /graphene composites with different mass ratio, (b) Raman spectra of Sample 1 and GO.
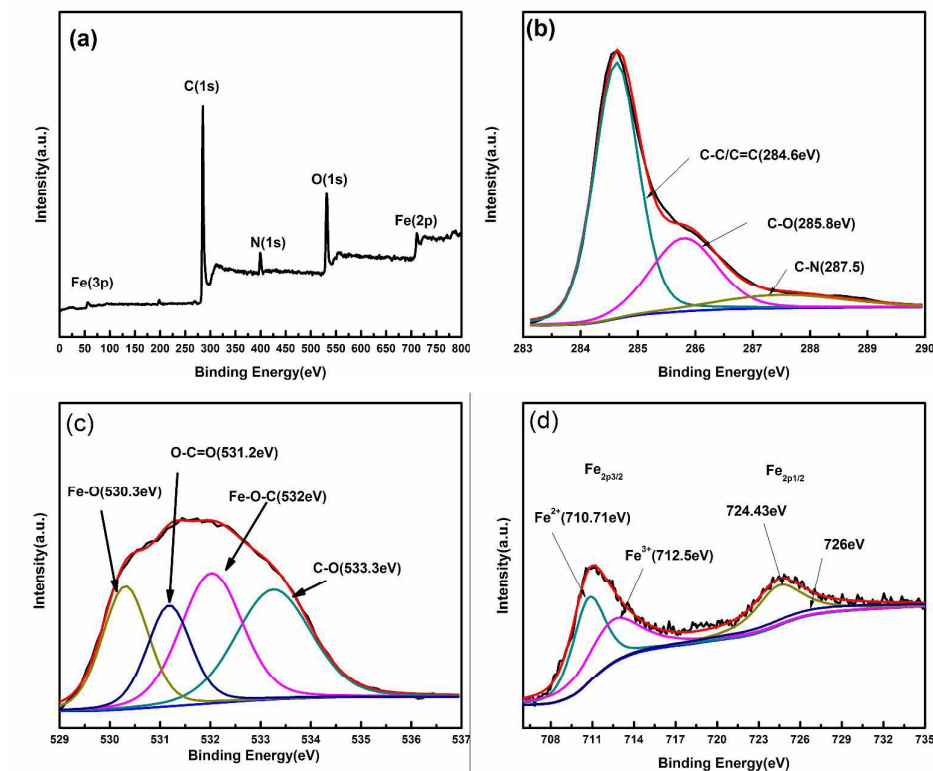
Fig.2- (a) XPS spectrum of Sample 1,(b) C_{1s}, (c) O_{1s} and (d) Fe_{2p} spectra of Sample 1
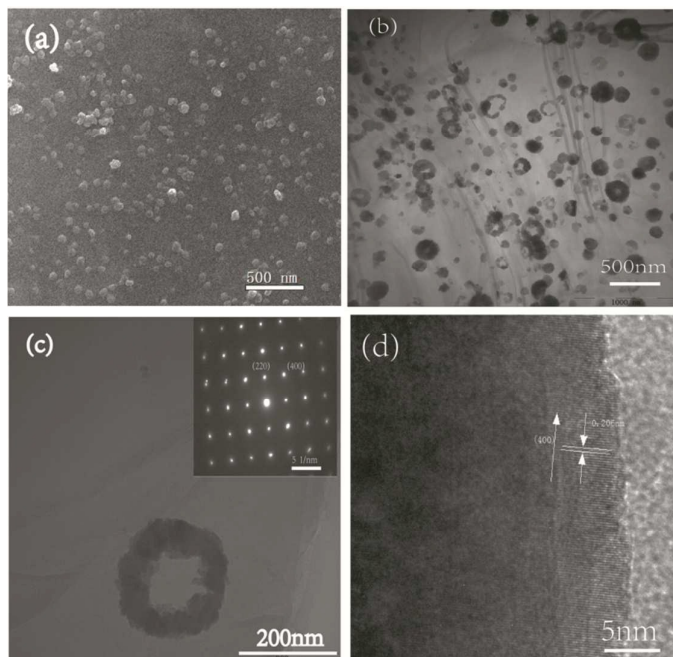
Fig.3-(a) SEM, (b) (c) TEM (d) HRTEM images of the composites Sample 1, the inset of (c)

shows the SAED pattern of Sample 1.
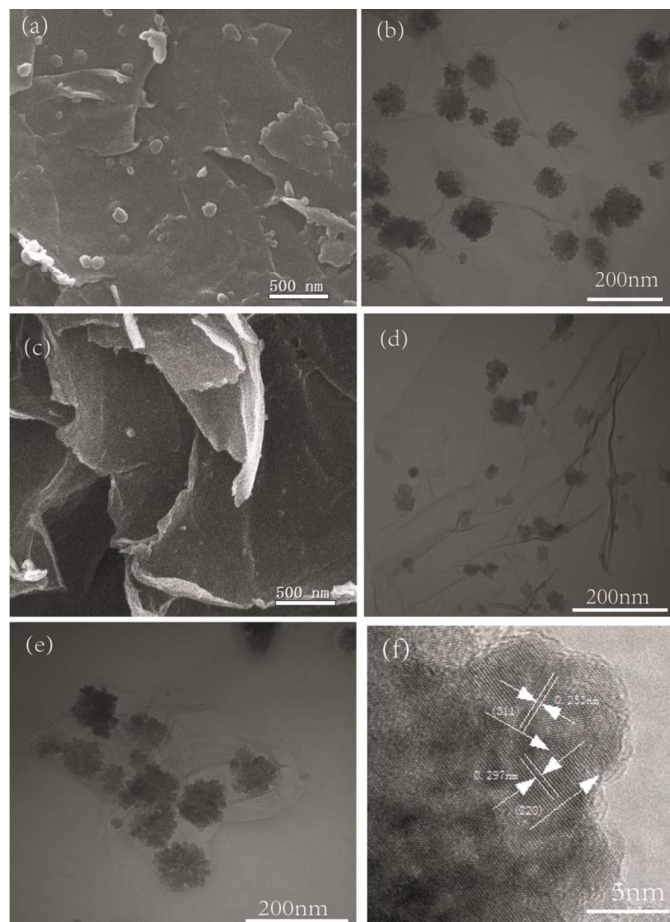
Fig.4-(a) SEM and (b)TEM image of Sample 2,(c) SEM and (d)TEM image of Sample 3, (e) TEM and (f) HRTEM images of the flower-like composites
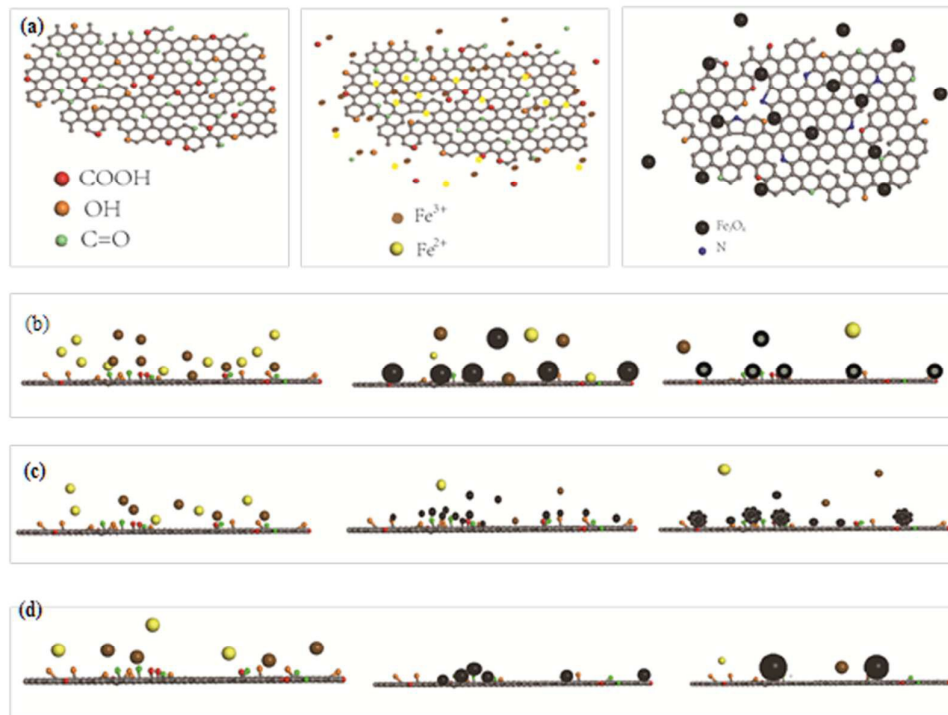
Fig. 5-(a) schematic view of the procedure of the as prepared Fe_3O_4 / graphene composite; the illustration of the composites fabrication process (b) Sample 1, (c) Sample 2 and Sample 3, (d) Sample 4.
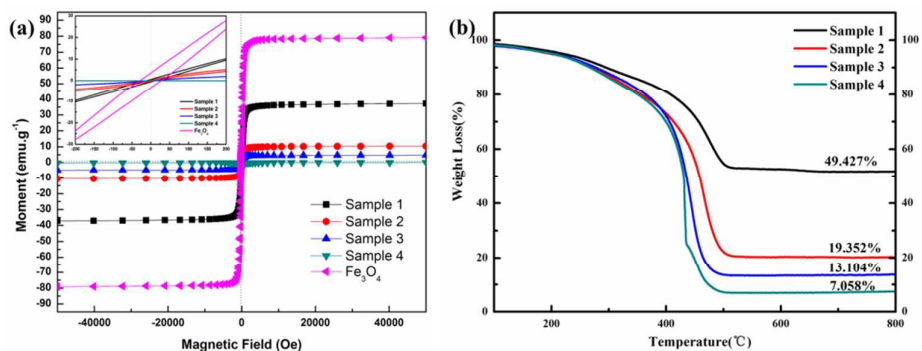
Fig.6-(a) Magnetization curves at room temperature of the pure Fe_3O_4 and Fe_3O_4 /graphene composites; (b) The TGA curves of prepared Fe_3O_4 / graphene composite
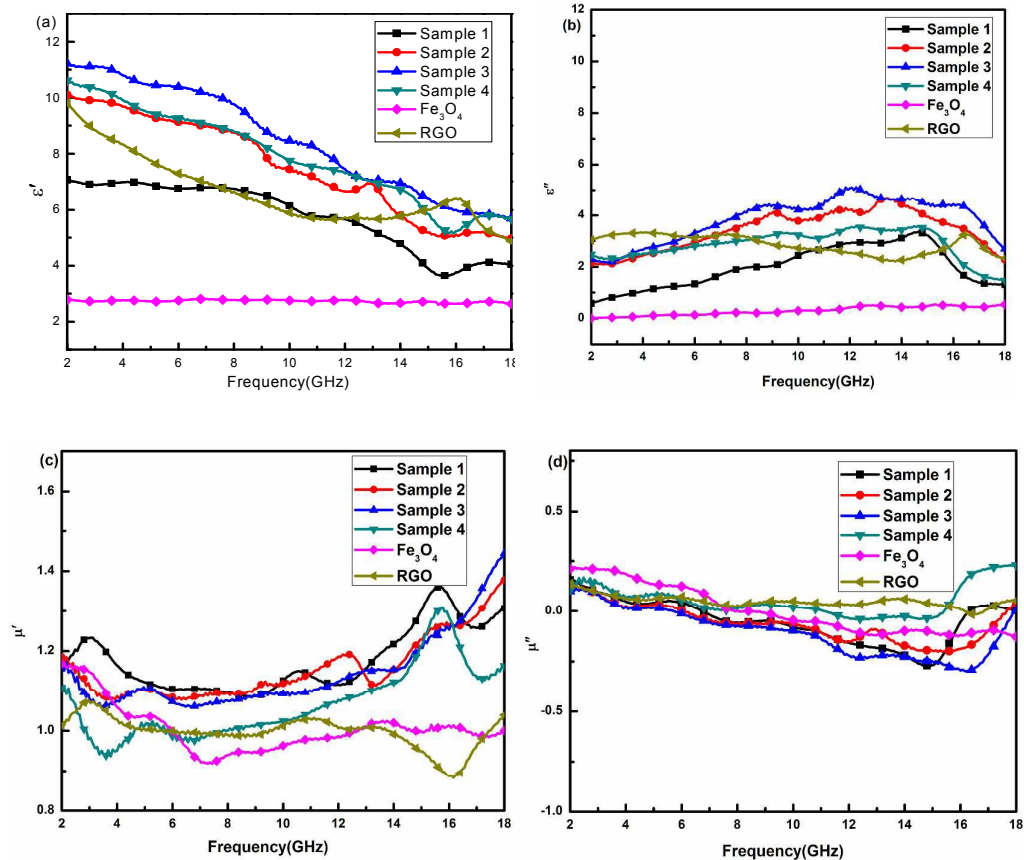
Fig. 7-Frequency dependence of (a) real and, (b) imaginary parts of complex permittivity, (c) real

parts and (d) imaginary parts of complex permeability of the Fe_3O_4 nanoparticles, graphene, and

Fe_3O_4 /graphene composites
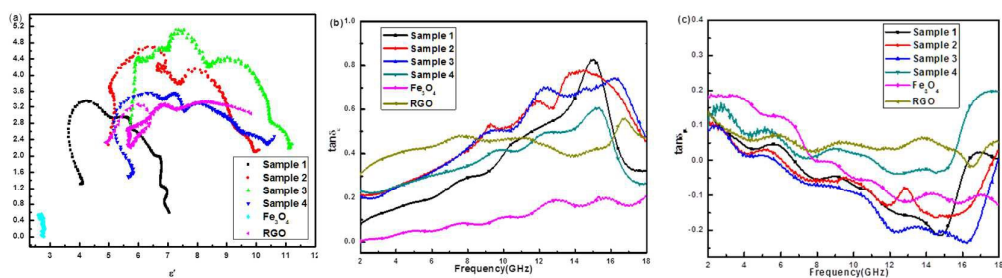
Fig.8- (a) typical Cole-Cole curves (b) dielectric loss factor and (c) magnetic loss factor of Fe_3O_4

nanoparticles, graphene and Fe_3O_4/graphene composites
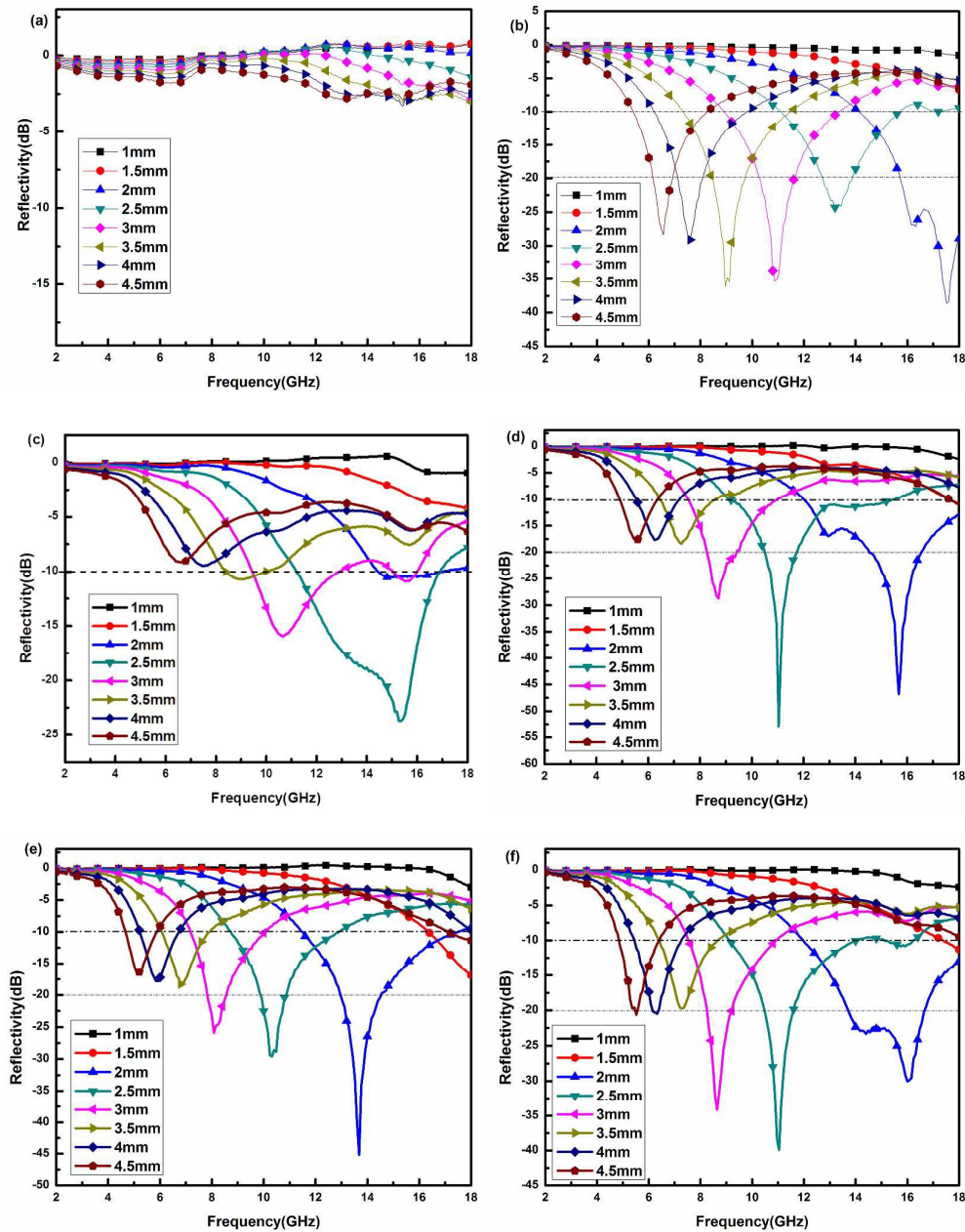
Fig.9- Reflection loss curves of (a) Fe_3O_4, (b) graphene, (c) Sample 1, (d) Sample 2, (e) Sample 3,

and (f) Sample 4 with different thicknesses
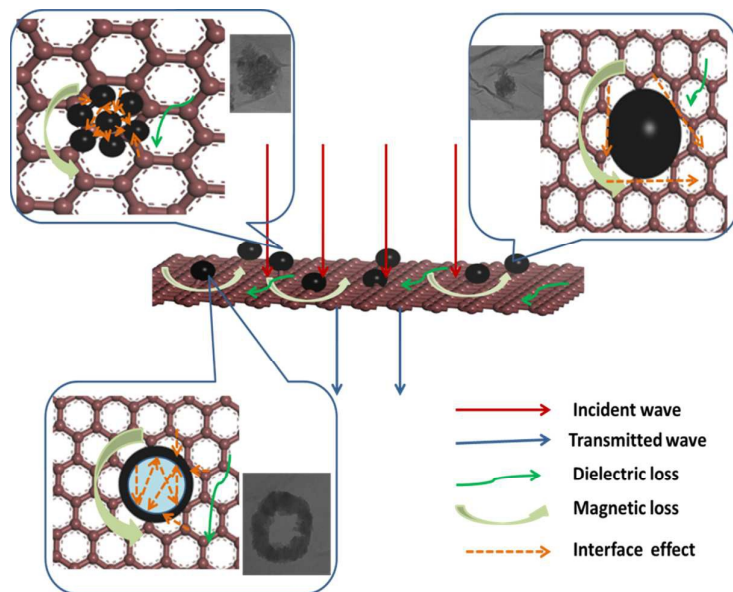
Fig.10- schematic view of the physical model for the composites with different morphology of

Fe_3O_4 nanoparticles

Table 1. The comparison of microwave absorption performance of Fe_3O_4 and composites

Sample	Max RL value(dB)	d(mm) (max RL value)	Frequency(GHz) (max RL value)	Frequency range(GHz)	Effective bandwidth	d(mm) (different frequency range)	Refs
Fe_3O_4 nanorods	-40	4.4	≈ 2.5				Ref[45]
Fe_3O_4 nanoparticles	-40	8.0	≈ 1	s			Ref [45]
hollow Fe_3O_4 nanoparticles	<-40	55 and 21	2.5 and 11.4	4~8 (RL≤-10dB)	4GHz	30.0	Ref[46]
Fe_3O_4 decorated single-wall carbon nanoborns	-38.8	5.8	3.7	3.2~12.4 (RL≤-10dB)	9.2GHz	2~6	Ref [11]
Polyaniline/graphene oxide/ Fe_3O_4	-53.5	3.9	7.5	6.4~9.2 (RL≤-10dB)	2.8GHz	3.9	Ref [48]
bowl-like Fe_3O_4 hollow spheres/reduced graphene oxide	-24.0	2.0	12.9	10.8~15.7 (RL≤-10dB)	4.9GHz	2.0	Ref [17]
reduced graphene oxide/Fe_3O_4 composite	-44.6	3.9	6.6	12.2~16.5 (RL≤-10dB)	4.3GHz	3.0	Ref [47]
Graphene-Fe_3O_4 nanohybrids	-40.4	5.0	7.0	5.1~14.6 (RL≤-15dB)	9.5GHz	2~5	Ref [44]
hollow Fe_3O_4 /graphene composite	-23.7	2.5	15.3	11~17 (RL≤-10dB)	6GHz	2.5	This work
flower-like Fe_3O_4/Graphene composites	-53.2	2.5	11.4	9~16 (RL≤-10dB)	7GHz	2.5	This work
solid sphere Fe_3O_4/Graphene composites	-40.0	2.5	11.0	9.12~16.25 (RL≤-10dB)	7.13GHz	2.5	This work
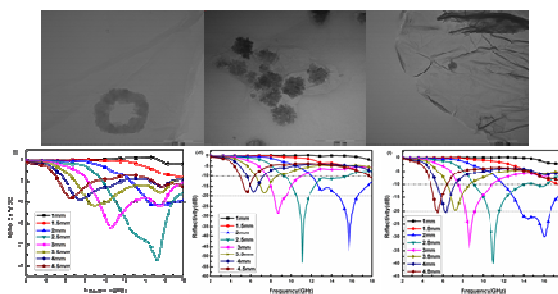
With the experimentally controlled structures from ring-like, flower-like to solid spheres for nanoparticles, the Fe$_3$O$_4$/graphene composites show excellent microwave absorption properties.